An investigation on galvanic corrosion in friction-stir-welded AA 5083 aluminum alloy

Eduardo Antunes Duda[1]
Sabrina da Silva Soares[1]
Diogo Trento Buzzatti[1]
Guilherme Vieira Braga Lemos[1,2*]
Tárique Hernandez Schneider[1]
Henrique Ribeiro Piaggio Cardoso[1]
Tiago Falcade[1]
Afonso Reguly[1]

Abstract

Friction-stir welding (FSW) is a well-known solid-state technology for manufacturing high-quality aluminum welds. However, corrosion may become an issue due to the changes in the microstructure within the stir zone, perhaps creating a local galvanic couple. In this work, AA 5083-O aluminum plates were joined by FSW, and corrosion analyzes were undertaken. Therefore, corrosion behavior was investigated using an immersion test, open circuit potential (OCP), and zero-resistance ammeter (ZRA) measurements. The stirred material was found to be more resistant to pitting nucleation than the AA5083-O alloy base material on immersion test and OCP analyzes. Nevertheless, deeper pits were more significant in the stirred material. The ZRA test showed similar results for both regions, indicating this system's low galvanic couple effect.

Keywords: Friction-stir welding; AA 5083-O; Corrosion; Immersion test; Open circuit potential; Zero-resistance ammeter.

1 Introduction

The use of aluminum for several applications has grown throughout the years. Thus, aluminum alloys to replace steel usually concern a high strength-to-weight ratio increasing the transport carrying capacity or less fuel consumption and decreasing CO_2 emission. The 5083-O alloy, among the several aluminum alloys, is employed in the aerospace, automotive, and naval industries due to its mechanical properties, low density, and good corrosion resistance [1].

The formation of porosities and cracks is typical in the fusion welding of aluminum alloys. Friction-stir welding (FSW), a low heat input manufacturing process, is recommended for these alloys [2]. Therefore, high-quality joints can be provided by FSW, a joining process of solid-state nature. Moreover, microstructural changes and grain coarsening may be prevented by its lower heat input and still result in a recrystallized microstructure [3]. FSW is used in various industrial applications, like automotive, naval, and high-speed train manufacturing [4-6]. A non-consumable tool plays an essential role in joining the workpieces, further achieving an improved joint quality since there is no melting of the materials. Moreover, due to its efficiency and less consumable energy, FSW is considered a green technology [3-7].

Friction stir welds of AA 5083 and the process parameters that influence their joint properties were studied by many authors [8-12]. Mishra and Rani [8] found that tool rotational speed is the most significant factor in decreasing joint elongation. Klobčar et al. [9] reported that the weld with excessive flash generation, grain growth, and lower hardness than the base material occurs due to high heat input. Rao et al. [10] studied the asymmetric distribution of microstructure and mechanical properties. It was found that the hardness sharply decreased from heat-affected zone (HAZ) to the stir zone (SZ) on the advancing side (AS). Prabha et al. [11] investigated the effects of tool rotational speeds of 900, 1120, 1400, and 1800 rpm at a welding speed of 40 mm/min. The best ultimate tensile strength (UTS) and finer microstructure were assessed using a tool rotational speed of 1120 rpm. Hirata et al. [12] applied different tool rotational and transverse speeds, which found that regardless of the condition, the UTS was almost the same, and the microstructure of the stir zone consisted of fine equiaxed grains. Therefore, a decrease in grain size resulted in a hardness increase in the SZ, which improved the mechanical properties of friction-stir-welded 5083 alloy.

The interface between the base material and stir zone generates a condition that could be prone to galvanic

[1] *Laboratório de Metalurgia Física, LAMEF, Universidade Federal do Rio Grande do Sul, UFRGS, Porto Alegre, RS, Brasil.*
[2] *Universidade Federal de Santa Maria, UFSM, Cachoeira do Sul, RS, Brasil.*

**Corresponding author: guilherme.lemos@ufrgs.br*

corrosion, owing to the risk of any welding process that induces microstructural changes. Although aluminum alloys have a passive layer, pitting corrosion could be severe in specific environments, especially those containing chloride ions [13,14]. Galvanic corrosion would take place when the base and stirred materials have a potential difference. The noblest is the cathode, and the anode is the most active (most susceptible to corrosion) [15]. In this investigation, it should be noted that the corrosion evaluation was performed on the top surface as this region is typically exposed to the environment where the related degradation phenomena might occur. Therefore, corrosion analyzes were carried out to assess the effect of galvanic couple. Thus, this work investigated the corrosion behavior of friction-stir-welded AA 5083-O.

2 Materials and methods

2.1 Materials

Friction-stir-welded AA 5083-O aluminum plates with 400 x 80 x 6.35 mm were investigated in this work. An AISI H13 steel tool with a shoulder of 18 mm diameter and probe length of 6 mm was used for solid-state welding. FSW was performed with a tool rotational speed of 1100 rpm and a welding speed of 30 mm/min [16]. The chemical composition measured in the base material is given in Table 1. Samples were cut using electrical discharge machining (EDM) according to the dimensions shown in Figure 1.

Electrochemical tests aimed to evaluate the galvanic couple between the base material (AA 5083-O) and the stirred material. Figure 2 shows the experimental arrangement for OCP and ZRA tests. Therefore, OCP was measured separately to evaluate corrosion in the as-received (base material) and stirred material. At the same time, the ZRA was used to evaluate the current between the base and stirred materials together as a galvanic pair. All electrochemical and immersion tests were carried out in a 5 mmol/L NaCl aerated solution at room temperature [17].

2.2 Methods

2.2.1 Sample preparation for corrosion analyzes

The samples were cold mounted in resin, grounded in sandpaper 80 to 1200 grit SiC papers, and polished with 4 µm and 1 µm diamond past. Then, they were cleaned with distilled water (96% alcohol), and dried with nitrogen.

2.2.2 Immersion test

This test was based on ASTM G46 [18] and ASTM G44 standards [19]; the sample comprised the base and stirred materials in 20 x 10 mm. The tests were carried out by continuous immersion for 1 and 24 hours. After each period, the samples were cleaned and dried. Before and after immersion, images were taken using a Leica DM2700 microscope to assess the surface. In addition, the samples were analyzed on a light interferometer Bruker-Contour GT-K for measuring the pit depths, and the appearance of new pits over the time. Thus, several images were taken using green light and 2.5x with a #2 field of view (FOV).

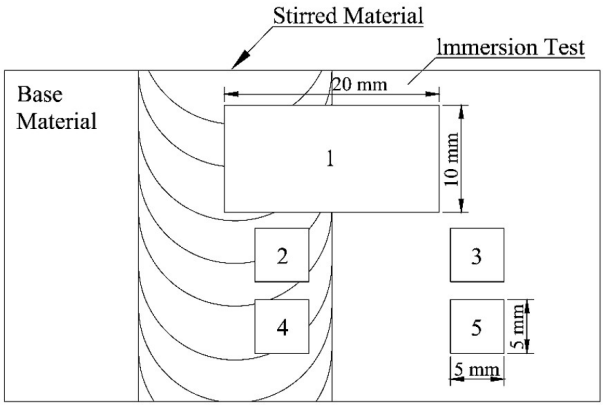

Figure 1. Schematic sketch of the samples in friction-stir welded AA 5083 alloy: #1 stands for immersion tests; #2 and #3 for OCP tests, and #4 and #5 for ZRA test.

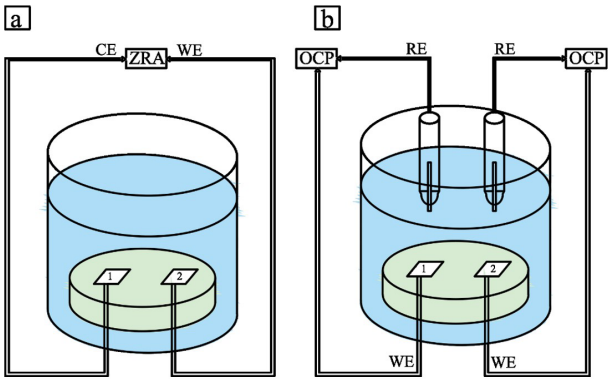

Figure 2. Experimental arrangement for ZRA and OCP tests. ZRA: a) the counter electrode (CE) of the zero resistance amperemeter was connected to the base material sample, and the working electrode (WE) was connected to the stirred one; OCP b) the potential of each sample was monitored concerning Ag/AgCl (3 mol/L KCl) reference electrode.

Table 1. Chemical composition of AA 5083-O aluminum alloy base material (% wt.)

	Al	Mg	Mn	Fe	Si	Zn	Cr	Ti	V	Cu
AA 5083-O	Bal.	4.89	0.53	0.33	0.18	0.087	0.075	0.014	0.011	0.008

2.2.3 Open Circuit Potential (OCP) and Zero Resistance Ammeter (ZRA)

Samples with 5 x 5 mm were embedded in acrylic resin (Figure 2), and their sides were insulated to avoid crevice corrosion. At first, the OCP and ZRA tests of base and stirred materials were measured for 24 hours. For these tests, conduced separately, an Ag/AgCl (3 mol/L KCl) was the reference electrode (RE) [20,21].

For the OCP, two potentiostats (an Autolab 302N Potentiostat – Metrohm and Gamry Potentiostat Interface 1000E) did the measurements, one for each sample (base and stirred materials without electric contact).

The ZRA measures the current between a galvanic pair [22], which technique was performed according to the ASTM G71 [23] and the Potentiostat Manual [24]. An Autolab 302 N Potenciostat – Metrohm was then used. In this context, the stirred material acts as a working electrode (WE), and the base material as the counter electrode (CE), so all ZRA data is reported concerning the stirred material. ZRA currents were normalized by each sample area, keeping a 1:1 proportion between the base and stirred materials. A smoothing filter with the FFT was further used.

3 Results and discussion

3.1 Immersion test

Interferometric images taken before and after immersion tests and these are shown in Figure 3. The color scale was normalized for comparing the surface profiles better. After 1st hour of immersion, some pits grew in both base and stirred material; in the latter, the density of deeper pits seems to be more prominent, while in the base material, smaller and shallower pits were dominant. Later, after 24 hours of immersion, a significant number of pits were evident in both materials compared to that of the one hour of immersion. Stirred material displayed greater number of deeper pits, whereas the base material showed greater density of smaller pits. Overall, concerning 24 hours of immersion, the base material showed more pits than the stirred one.

The trend noted in the 24 hours of immersion corroborates well with interferometric analysis (see Figure 4), where the base material had the worst condition. All the pits below 0.2 µm depth and 6.4 µm diameter were disregarded to eliminate noises and small previous defects. For comparison purposes, the same procedure was done in the sample before immersion. In this case, the total pit density was less than 50 pits/cm^2 for base and stirred materials, which is relatively less than the values reached after immersion. Thus, considering 1 hour of immersion, around 1640 pits/cm^2 and 1950 pits/cm^2 were verified in the base and stirred materials, respectively. For 24 hours of immersion, approximately 9830 pits/cm^2 and 9550 pits/cm^2 were achieved in the base and stirred materials, respectively.

Figure 4 shows the base material that had a more significant number of shallow pits (less than 0.7 µm). Interestingly, the pit density decreases for higher pit depths, suggesting that the nucleation is more prominent than growth in the base material. On the other hand, stirred material showed a greater number of deeper pits (above 0.7 µm). This behavior is even more distinguishable for the deepest pits (greater than 0.9 µm). Therefore, stirred material showed around four times more pits/cm^2 than the base material, regardless of the immersion time, indicating that the pit growth is, to some extent, more important in this region.

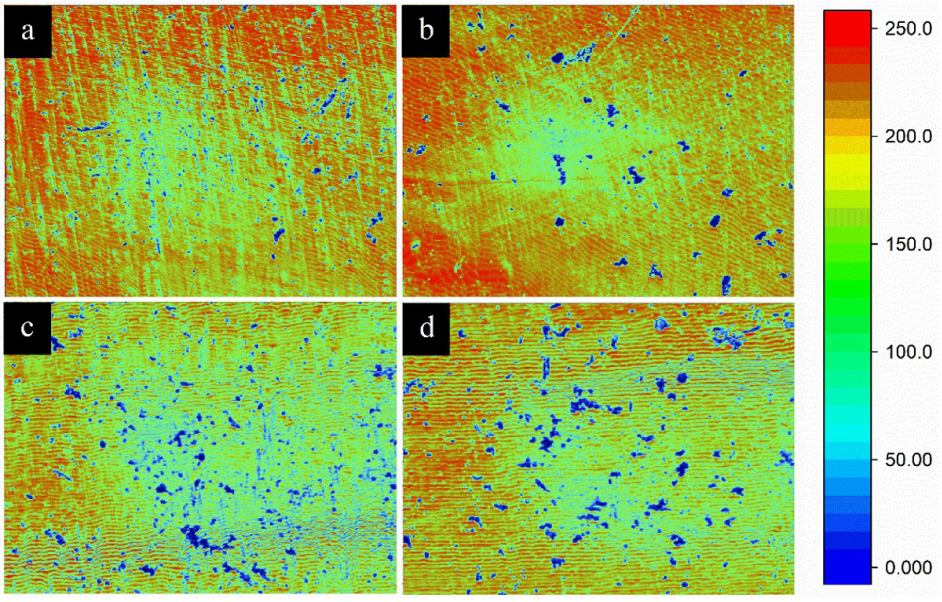

Figure 3. Optical microscopy after immersion tests in NaCl 5mmol/L aerated at various exposure times. 1h of immersion test: a) base material, b) stirred material; 24h of immersion test: c) base material, d) stirred material. The area of each image is 0.97 mm x 1.3 mm

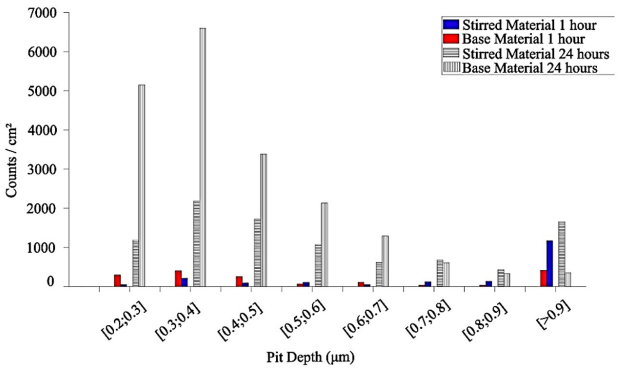

Figure 4. Histogram of pitting density versus pit depth after immersion tests in NaCl 5mmol/L aerated at various exposure times: 1 hour and 24 hours.

Before immersion, the mean roughness measured by interferometry was of around 30.6 ± 8.8 nm and 20.4 ± 4.3 nm for the base and stirred materials, respectively. After 24 hours of immersion, the roughness changed to 79.9 ± 16.7 nm for the base material and 64.6 ± 5.4 nm for the stirred one. Thus, in general, the mean roughness increased three times for both materials, which is expected due to the pitting formation.

3.2 Open Circuit Potential

A representative curve of OCP evolution for 24 hours for the base material and stirred material is shown in Figure 5a. Initially, OCP values (base and stirred materials) increased rapidly, followed by a slower decrease until a stationary value after around 16 hours of immersion. Besides, the potential was similar for both regions, showing differences of around 50 mV, which might be related to low susceptibility to galvanic corrosion of AA5083 alloy [25].

The potential varies for a surface alteration (e.g., formation and breakage of the passive layer [26]). A tendency of change was noted for the nobler potential in the first hours of test followed by a drop to more negative values. Thus, the potentials for the first hours can be associated with the passive layer [27,28]. The next change to further negative potentials suggests that the passive layer was unsuitable for resisting corrosion in 5 mmol/L NaCl.

The behavior seen in Figure 5b is an indication of the breakdown of the passive layer, thus inducing a pitting process [28].

On the surface, there might be sites susceptible to chloride attack (inclusions, heterogeneities, and second-phase particles [29]); these regions may act as preferential sites for nucleation of pits. The breakage of the passive layer would cause the potential to shift to more negative values, indicating development of active sites. After repassivation, the potential returns to the previous level. This passivation effect is more frequent in the base material than in the stirred one, which corroborates with the more prominent nucleation

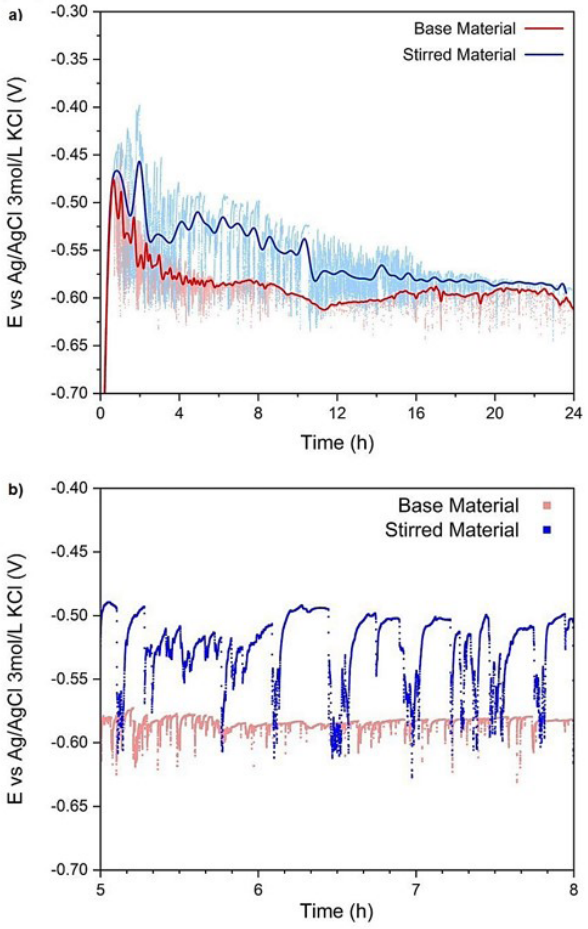

Figure 5. a) Open circuit potential transient for AA 5083-O base material and stirred material in NaCl 5mmol/L aerated using a smoothing filter with the FFT. b) Effect of the breakage of the passive layer and repassivation in AA5083 (base and stirred materials).

in the base material after 24 hours of immersion. In Figure 5a, more pronounced potential drops may indicate deeper pits (stirred material), which can also be seen in Figure 5b since the number of deeper pits was remarkable in this region.

3.3 Zero Resistance Ammeter

The representative curve of ZRA evolution in the 24 hours for the galvanic pair is shown in Figure 6. The noise at the beginning of the test could represent the breakage of the passive layer in the base or the stirred materials, and thus a pitting corrosion [17]. However, it was not possible to define in which sample this phenomenon occurred first.

Liu et al. [30] presented a similar behavior of current density in ZRA analysis for magnesium alloy. The experimental data plotted here references the stirred material so that the negative currents indicate the cathode, and the base material is the anode. Moreover, it seems that a shift in the current direction is due to the initial surface stabilization as seen in OCP measurements, which showed similar values for both regions.

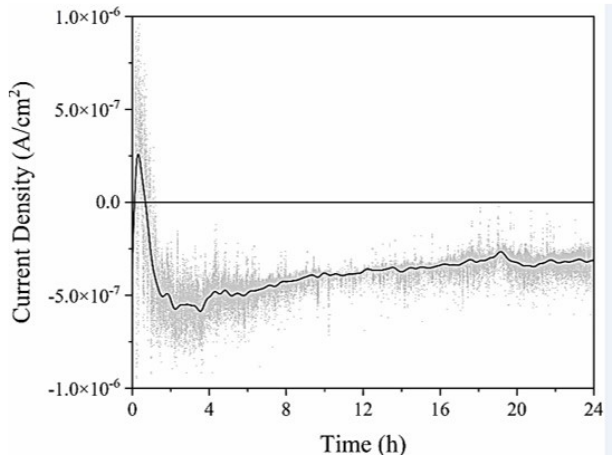

Figure 6. ZRA analysis on AA 5083 base and stirred materials during 24 hours in NaCl 5mmol/L aerated solution using a smoothing filter with the FFT. Current density is reported concerning stirred material, which acts as t=he working electrode. In turn, the base material is the counter electrode, and its current density has the same magnitude but opposite direction.

The OCP decreased throughout the potential stabilization of the base material, which was consistently lower than that of the stirred material, resulting in negative current density, as shown in Figure 6. The maximum cathodic current density occurred for 3 to 4 hours of immersion. Later, this density became less negative, agreeing well with the OCP behavior that showed a smaller difference between the base and stirred materials for longer immersion times (around 16 hours). As the potential difference between the base material and the stirred is moderate, the galvanic current also has small values. Thus, the trend verified herein indicates that the stirred material has a slightly more noble behavior than the base material.

Although the current density for the stirred material was slightly negative for almost the whole time, both regions developed certain corrosion. This was evidenced by the pitting corrosion noted in Figure 4, which is explained by the shift between the cathode and anode potential.

4 Conclusions

i) The stirred material in friction-stir welded AA 5083 aluminum alloy presents a certain resistance to nucleation of small pits, as verified in the immersion test. However, deeper pits were present in more amount in this region, in which these surface defects could be deleterious for mechanical properties.

ii) The OCP showed few differences in the electrochemical potential for these regions, where the stirred became less prone to corrosion, and the pit nucleation was more intense in the base material. So, even though both materials suffered continuous corrosion during 24 hours of immersion, the small galvanic effect induced, to some extent, certain protection to the stirred material.

iii) ZRA test further proved that the stirred material is nobler than the base material, but a considerable galvanic effect was not observed. Overall, FSW showed an acceptable electrochemical coupling referring to galvanic corrosion.

Acknowledgements

We would like to acknowledge the support of Fundação de Amparo à Pesquisa do Estado do Rio Grande do Sul (FAPERGS).

References

1 Tronci A, McKenzie R, Leal RM, Rodrigues DM. Microstructural and mechanical characterisation of 5XXX-H111 friction stir welded tailored blanks. Science and Technology of Welding and Joining. 2011;16(5):433-439.

2 Thakur R, Bajwa PS. Friction stir welding of 5xxx series aluminium alloys : a literature survey. International Journal of Scientific Research in Science, Engineering and Technology. 2016;2(2):1129-1131.

3 Mishra RS, Ma ZY. Friction stir welding and processing. Materials Science and Engineering R Reports. 2005;50(1–2):1-78.

4 Çam G. Friction stir welded structural materials: beyond Al-alloys. International Materials Reviews. 2011;56(1):1-48.

5 Hori H, Hino H. Application of friction stir welding to the car body. Welding International. 2003;17(4):287-292.

6 Stephan W, Kallee, EDN, Burling PM. Application of friction stir welding for the manufacture of aluminium ferries. In: 4th International Forum on Aluminium Ships. New Orleans: NIES; 2000.

7 Li Y, Trillo EA, Murr LE. Friction-stir welding of aluminum alloy 2024 to silver. Journal of Materials Science Letters. 2000;19(12):1047-1051.

8 Mishra RS, Rani P. Experimental investigation of joining of aluminum alloy 5083 by friction stir welding (FSW). IJREI. 2019;3(5):306-309.

9 Klobčar D, Kosec L, Pietras A, Smolej A. Friction-stir welding of aluminium alloy 5083. Materials Technology. 2012;46(5):483-488.

10 Rao D, Huber K, Heerens J, dos Santos JF, Huber N. Asymmetric mechanical properties and tensile behaviour prediction of aluminium alloy 5083 friction stir welding joints. Materials Science and Engineering A. 2013;565:44-50.

11 Prabha KA, Putha PK, Prasad BS. Effect of tool rotational speed on mechanical properties of aluminium alloy 5083 weldments in friction stir welding. Materials Today: Proceedings. 2018;5(9):18535-18543.

12 Hirata T, Oguri T, Hagino H, Tanaka T, Chung SW, Takigawa Y, et al. Influence of friction stir welding parameters on grain size and formability in 5083 aluminum alloy. Materials Science and Engineering A. 2007;456(1–2):344-349.

13 Szklarska-Smialowska Z. Pitting corrosion of aluminum. Corrosion Science. 1999;41(9):1743-1767.

14 Aballe A, Bethencourt M, Botana FJ, Cano MJ, Marcos M. Influence of the cathodic intermetallics distribution on the reproducibility of the electrochemical measurements on AA5083 alloy in NaCl solutions. Corrosion Science. 2003;45(1):161-180.

15 Segaetsho MOM, Msomi V, Moni V. Corrosion behaviour of friction stir welded dissimilar joints produced from AA5083 and other alloys of aluminium: a critical review. Materials Today: Proceedings. 2022;56:1696-1701.

16 Brum N, Amavisca C, Schroeder JG, Buzzatti J, Lemos GVB, Tolotti D, et al. Influence of process parameters on mechanical properties of friction stir welded 5083-O aluminum alloy. Tecnologica em Metalurgia, Materiais e Mineração. 2021;18:e2450.

17 Kartsonakis IA, Dragatogiannis DA, Koumoulos EP, Karantonis A, Charitidis CA. Corrosion behaviour of dissimilar friction stir welded aluminium alloys reinforced with nanoadditives. Materials & Design. 2016;102:56-67.

18 ASTM G01 Committee. ASTM G46: guide for examination and evaluation of pitting corrosion. USA: ASTM International; 2005 [cited 2022 June 20]. Available at: http://www.astm.org/cgi-bin/resolver.cgi?G46-94R18

19 ASTM G01 Committee. ASTM G44: standard practice for exposure of metals and alloys by alternate immersion in neutral 3.5% sodium chloride solution. USA: ASTM International; 2021.

20 Inzelt G, Lewenstam A, Scholz F. Handbook of reference electrodes. Dordrecht: Springer; 2013.

21 Smith TJ, Stevenson KJ. Reference electrodes. In: Zoski CG, editor. Handbook of electrochemistry. Amsterdam: Elsevier; 2007 [cited 2022 June 20]. p. 73–110. Available at: https://www.sciencedirect.com/science/article/pii/B9780444519580500057

22 Espallargas N, Johnsen R, Torres C, Muñoz AI. A new experimental technique for quantifying the galvanic coupling effects on stainless steel during tribocorrosion under equilibrium conditions. Wear. 2013;307(1–2):190-197.

23 ASTM G01 Committee. ASTM G71: guide for conducting and evaluating galvanic corrosion tests in electrolytes. USA: ASTM International; 2014 [cited 2022 June 20]. Available at: http://www.astm.org/cgi-bin/resolver.cgi?G71-81R14

24 Metrohm. NOVA User Manual. Netherlands: Metrohm; 2017.

25 Hack HP. Galvanic corrosion. Philadelphia, PA: ASTM; 1988. 358 p.

26 Zaid B, Saidi D, Benzaid A, Hadji S. Effects of pH and chloride concentration on pitting corrosion of AA6061 aluminum alloy. Corrosion Science. 2008;50(7):1841-1847.

27 El-Dahshan ME, Shams El Din AM, Haggag HH. Galvanic corrosion in the systems titanium/316 L stainless steel/Al brass in Arabian Gulf water. Desalination. 2002;142(2):161-169.

28 Tomcsányi L, Varga K, Bartik I, Horányi H, Maleczki E. Electrochemical study of the pitting corrosion of aluminium and its alloys—II. Study of the interaction of chloride ions with a passive film on aluminium and initiation of pitting corrosion. Electrochimica Acta. 1989;34(6):855-859.

29 Moreto JA, Marino CEB, Bose Filho WW, Rocha LA, Fernandes JCS. SVET, SKP and EIS study of the corrosion behaviour of high strength Al and Al–Li alloys used in aircraft fabrication. Corrosion Science. 2014;84:30-41.

30 Liu J, Han E, Song Y, Shan D. Effect of twins on the corrosion behavior of Mg–5Y–7Gd–1Nd–0.5Zr Mg alloy. Journal of Alloys and Compounds. 2018;757:356-363.

Received: 20 June 2022
Accepted: 17 Nov. 2022